

Modeling intermolecular Coulombic decay with non-Hermitian real-time time-dependent density functional theory

Yi-Siang Wang, James X. Zhong Manis, Matthew C. Rohan, Thomas M. Orlando, and Joshua S. Kretchmer*

School of Chemistry and Biochemistry, Georgia Institute of Technology, Atlanta, GA 30332, USA

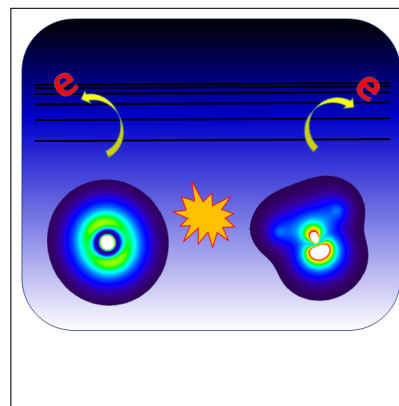
E-mail: jkretchmer@gatech.edu

Abstract

In this work, we investigate the capability of using real-time time-dependent density functional theory (RT-TDDFT) in conjunction with a complex absorbing potential (CAP) to simulate the intermolecular Coulombic decay (ICD) processes following the ionization of an inner-valence electron. We examine the ICD dynamics in a series of non-covalent bonded dimer systems, including H₂O-H₂O, HF-HF, Ar-H₂O, Ne-H₂O and Ne-Ar. We consider an initial state generated from an inner-valence excitation on either monomer within each dimer, as the monomers are symmetrically not equivalent. In comparison to previous RT-TDDFT studies, we show that RT-TDDFT simulations with a CAP correctly capture the ICD phenomenon in systems exhibiting a stronger binding energy. The calculated time-scales for ICD of the studied systems are in the range of 5-50 fs in agreement with previous studies. However, there is a break-down in the accuracy of the methodology for the more weakly bound, pure van der Waals bonded systems. The accuracy in the former is attributed to both the use of the CAP and the choice of a long-range corrected functional with diffuse basis functions. The benefit of the presented real-time methodology is that it provides direct time-dependent population information without ne-

cessitating any *a-priori* assumptions about the electronic relaxation mechanism. As such, the RT-TDDFT/CAP simulation protocol provides a powerful tool to differentiate between competing electronic relaxation pathways following inner-valence or core ionization.

TOC Graphic



Keywords

density functional theory, complex absorbing potential, intermolecular Coulombic decay, real-time electronic structure, electron dynamics

The ionization of an inner valence or core electron can initiate competing electronic relaxation pathways that occur on an ultra-fast timescale, such as Auger-Meitner, intermolecular Coulombic decay (ICD), and electron-transfer mediated decay (ETMD) processes.¹⁻³ These processes play an important role in surface-science fragmentation and biological systems;^{4,5} the initial electron dynamics governs the subsequent fragmentation product distribution due to the Coulomb explosion of charged species in close proximity. In general, the majority of theoretical analysis of such processes has relied on static electronic structure calculations involving analyzing the ionization spectrum,⁶⁻⁸ density of states,⁹ or the broadening of the electronic states through non-Hermitian techniques.¹⁰⁻¹²

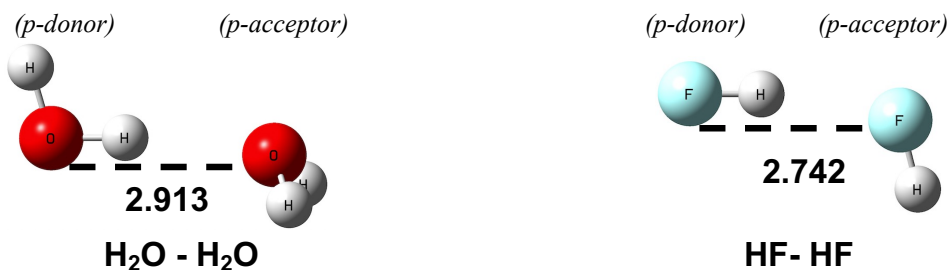
However, with the advent of attosecond spectroscopy, it is now possible to have experimentally time-resolved observation of ultra-fast processes with sub-femtosecond resolution.¹³⁻¹⁵ Therefore, there is a benefit to develop practical simulation methods that go beyond static techniques and can more directly report on such experiments. Real-time electronic structure methods, that directly solve for the time-propagation of the electronic wavefunction, provide a powerful class of techniques to accomplish such a goal.¹⁶⁻³⁸ In the context of electronic relaxation dynamics, a few highly accurate real-time studies have been performed on small systems, such as using the wave packet propagation method to simulate ICD in the Ne-Ar system³⁹ and *ab-initio* dynamical calculations to simulate acetylene dimer systems.⁴⁰ Additionally, a few studies have used RT-TDDFT with various levels of success.⁴¹⁻⁴⁷

In this work, we develop a practical simulation protocol to use RT-TDDFT to simulate the real-time ICD dynamics following an inner-valence ionization event. The ICD process involves initial ionization of a low lying electronic level. The hole left behind is filled from an electron in a higher lying electronic level on the same molecule. The energy released from this relaxation process is transferred to a neighboring molecule to ionize that molecule.³ In comparison to previous work, we employ a CAP

to account for the ionized secondary electron and a tuned long-range corrected functional with diffuse basis functions to accurately capture the dynamics. Figure 1 presents the variety of different dimer systems we examine including both hydrogen-bonded and pure van der Waals bonded systems. The nuclear geometry for each dimer was obtained from the global minimum at the CCSD(T) level of theory from the corresponding references: H₂O-H₂O,⁴⁸ HF-HF,⁴⁹ Ar-H₂O,⁵⁰ Ne-H₂O,⁵⁰ and Ne-Ar.⁵¹ Each dimer is asymmetric, either due to involving two different species or due to the asymmetric hydrogen-bonding geometry in the case of H₂O-H₂O and HF-HF. Therefore, to designate the two molecules in H₂O-H₂O and HF-HF we label one molecule as p-donor and one as p-acceptor corresponding to the hydrogen-bonding donor and acceptor in the dimer. As will be discussed, we examine the electron relaxation dynamics following the inner-valence ionization of each molecule in the dimers.

We perform the following procedure to initialize the electronic system to account for the initial inner-valence ionization. First, we perform a ground-state DFT calculation using the CCSD(T) geometries provided in Fig. 1. These calculations, as well as the subsequent real-time calculations, are performed using LC-PBE*,⁵² where the * indicates that we tune the range-separation parameter. Previous work has illustrated the importance of using a long-range corrected functional, or at least some amount of exact exchange, to appropriately account for charge dynamics.^{44,53,54} We use the aug-cc-pVDZ basis⁵⁵ for the molecule which will contain the initial hole (the trigger molecule), while the d-aug-cc-pVDZ⁵⁶ is used for the molecule that will be ionized during the ICD process (the target molecule). However, given that the d-aug-cc-pVDZ basis does not exist for Ar, we instead use the def2-TZVPPD⁵⁰ basis for the Ne-Ar system. We find that it is necessary to incorporate extra diffuse functions on the target molecule to more accurately describe the secondary ionization, though it is unnecessary to include the larger basis on the trigger molecule. Second, we generate the initial hole in the desired molecular orbital (MO) by man-

Hydrogen Bonded Systems



Non-Hydrogen Bonded Systems

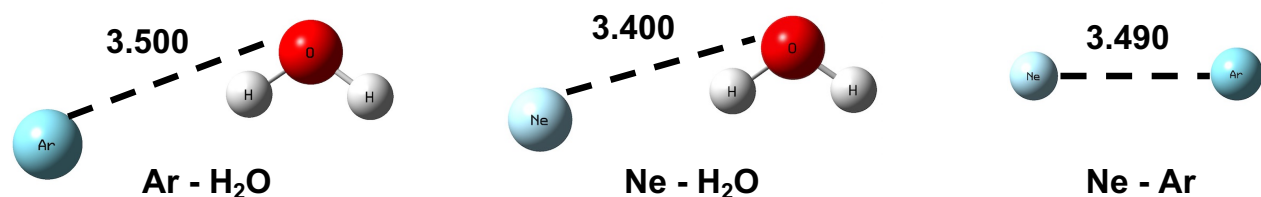


Figure 1: The geometry of the dimer systems investigated in this work including hydrogen-bonded (top) and non-hydrogen bonded (bottom) dimers. The heavy-atom internuclear distances are shown in Å. The monomers within the hydrogen-bonded dimers are designated as either proton donor (p-donor) or proton acceptor (p-acceptor) based on the geometry.

ually changing the occupancy of that orbital in the 1-electron reduced density matrix (1RDM) obtained from the ground-state calculation; we find that the inner-valence MOs are well localized in all cases making this choice relatively unambiguous. Full details of this procedure, including how we tune the range-separation parameter within LC-PBE*, and an investigation into our choice of functional and basis, are provided in the SI.

The real-time dynamics following the initial inner-valence ionization are simulated using RT-TDDFT as implemented in the NWChem⁵⁷ simulation package. One of the main difficulties in performing this simulation is how to appropriately account for the ionization of the secondary electron in a finite basis. To overcome this difficulty, we use a CAP to effectively remove the electron from the system as has been done to alleviate some of the numerical artifacts observed when simulating spectroscopy using real-time DFT.^{47,53} The modified RT-TDDFT

equations of motion are given as,

$$i\frac{\partial \mathbf{P}'(t)}{\partial t} = \mathbf{F}'(t)\mathbf{P}'(t) - \mathbf{P}'(t)\mathbf{F}'^\dagger(t) \quad (1)$$

where $\mathbf{P}'(t)$ is the 1RDM and $\mathbf{F}'(t)$ is a modified non-Hermitian DFT Fock matrix,

$$\mathbf{F}'(t) = \mathbf{F}'_0(t) + i\mathbf{\Gamma}'(t). \quad (2)$$

The prime notation indicates that the matrices are defined in the basis of orthogonalized atomic orbitals (AOs); the relation to the density matrix, \mathbf{P} , and Fock matrix, \mathbf{F} , in the standard AO basis are given through the procedure of canonical orthogonalization.^{58,59}

The damping matrix $\mathbf{\Gamma}'(t)$ is obtained from a time-independent diagonal damping matrix \mathbf{D} ^{47,53}

$$\mathbf{\Gamma}'(t) = \mathbf{C}'(t)\mathbf{D}\mathbf{C}'(t)^\dagger, \quad (3)$$

where $\mathbf{C}'(t)$ corresponds to the eigenvectors of the time-dependent Fock matrix in the orthogonalized AO basis, $\mathbf{F}'(t)$. The diagonal matrix \mathbf{D} contains exponentially increasing damping pa-

rameters (γ), such that

$$\gamma_i = \begin{cases} 0, & \text{if } \varepsilon_i - \varepsilon_0 < 0 \\ \gamma_0 e^{-\xi(\varepsilon_i - \varepsilon_0)}, & \text{if } \varepsilon_i - \varepsilon_0 > 0 \end{cases} \quad (4)$$

To obtain the specific values for the terms γ_0 , ζ , and ε_0 used to define the strength of the damping matrix, we follow an analogous protocol as employed in the context of spectroscopic calculations.^{47,53} Full details for the choice of these parameters along with the final values are provided in the SI.

We analyze the real-time dynamics in terms of (i) the occupancy of the MOs and (ii) the charge-loss on each monomer. One difficulty arises in the former in that ICD is normally described in terms of a local molecular orbital picture. However, the valence molecular orbitals tend to be delocalized across both monomers. Therefore, to analyze the electron relaxation dynamics we rotate the time-dependent 1RDM into the basis of ground-state MOs of each isolated monomer, such that

$$\tilde{\mathbf{P}} = \tilde{\mathbf{C}}^\dagger \mathbf{S} \mathbf{P} \mathbf{S} \tilde{\mathbf{C}}. \quad (5)$$

The matrix \mathbf{S} , is the overlap matrix of the AOs, and $\tilde{\mathbf{C}}$ contains the MOs of each isolated monomer following an orthogonalization procedure as performed through NWChem’s “NOSCF” routine.

The charge-loss on each monomer is defined as

$$\text{Charge loss on } A = N_{neutral}^A - \sum_{i=1 \in A}^{HOMO} \tilde{P}_{ii} \quad (6)$$

where the sum runs over the MOs associated with monomer A . The sum is truncated at the HOMO associated with the original ground-state of each monomer and $N_{neutral}^A$ corresponds to the total number of electrons on neutral monomer A . This choice of truncation has minimal impact on the observed results and is employed to minimize features arising with the choice of the CAP parameters.

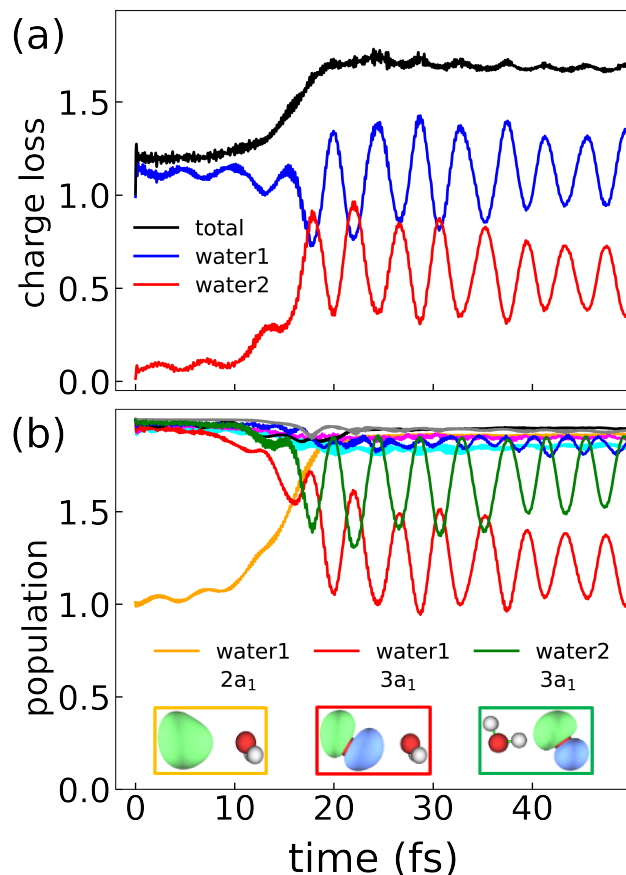


Figure 2: (a) The time-dependent charge-loss, Eq. (6), on the water 1 (blue) and water 2 (red) monomers, which correspond to the p-donor and p-acceptor, respectively. The total charge-loss of the H₂O-H₂O dimer (black) corresponds to the sum of the blue and red curves. (b) The time-dependent population of the MOs in the isolated monomer basis, Eq. (5). (water1 2a₁: orange, water1 1b₁: cyan, water1 1b₂: magenta, water2 2a₁: black, water2 1b₁: blue, water2 1b₂: grey, water2 3a₁: green) Insets show images of the MOs that are the dominant participants in the observed ICD mechanism. The orbitals are plotted using Multiwfn.⁶⁰

We now turn our attention to the results generated using the RT-TDDFT workflow described above. Figure 2 presents the real-time dynamics for the H₂O dimer following initial ionization from the 2a₁ MO on the p-donor (designated as water 1), which triggers a secondary ionization on the p-acceptor (designated as water 2). Figure 2(a) presents the total charge-loss (black), along with the charge-loss on water 1 (blue) and water 2 (red), Eq. (6).

The figure illustrates that initially, water 1 is in a cationic state, while water 2 is neutral. Water 2 then begins to lose charge at the same rate as the total system loses charge, while water 1 remains neutral. This is consistent with an ICD mechanism, indicating that our RT-TDDFT methodology is capable of successfully capturing the ICD process. The total charge-loss process occurs on the order of 20 fs, following which the charge on water 1 and water 2 begins to oscillate back and forth. The time-scale is in agreement with previous estimates of the ICD process in the literature.² The total charge-loss saturates at a value of ~ 1.6 , which is below the expected final value of 2. However, given both the approximate nature of the dynamics and the presence of the CAP, a perfect final value of 2 is not expected and we consider the observed value of 1.6 a success.

We can further examine the mechanism of the electronic decay process by analyzing the RT-TDDFT trajectories in more detail. Figure 2(b) presents the time-dependence of the MO occupation numbers in the isolated monomer basis, \bar{P}_{ii} . An initial hole is generated in the $2a_1$ MO on water 1 (orange), which is re-populated by an electron relaxing from the valence $3a_1$ MO on water 1 (red). Simultaneously, the water 2 valence $3a_1$ (green) MO lose electron density associated with ionization out of the MO. This physical picture observed by the real-time dynamics is completely consistent with the expected ICD mechanism in the water dimer. Furthermore, the time-scale of this whole process occurs on the order of 20 fs in agreement with Fig. 2(a). Following, the initial ICD process, we observe that the charge transfer pictured in part (a) is mainly associated with charge transfer between the water 1 $3a_1$ and water 2 $3a_1$ MOs.

We illustrate one of the main benefits of a real-time investigation into electron relaxation dynamics by also discussing the results on the Ar-H₂O system in detail, Fig. 3. In this system, the initial hole is generated on the Ar 3s orbital and the water molecule is ionized during the ICD process. Figure 3(a) plots the charge-loss on Ar (blue) and water (red). The general behavior, in which the Ar molecule remains

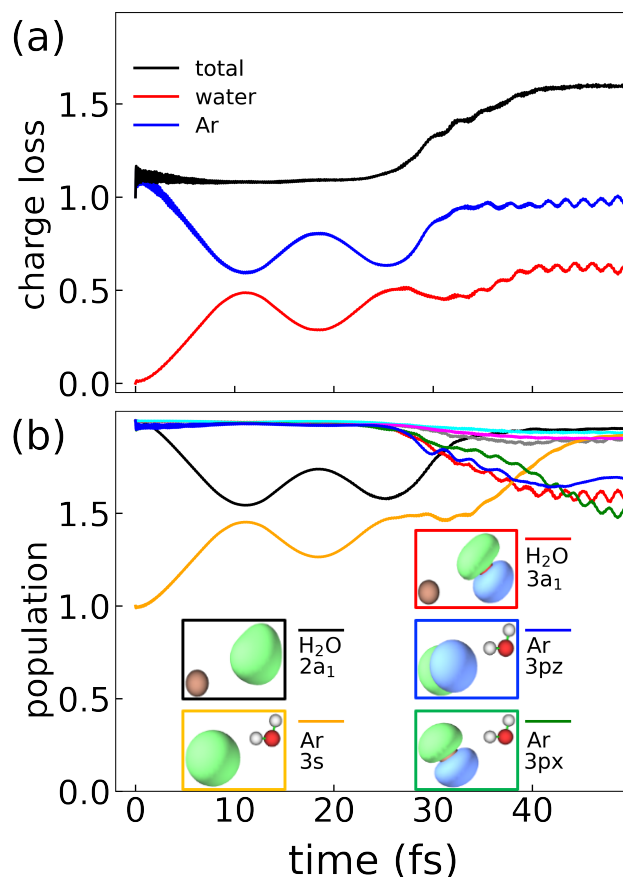


Figure 3: (a) The time-dependent charge-loss, Eq. (6), on Ar (blue) and water (red). The total charge-loss of the Ar-H₂O dimer (black) corresponds to the sum of the blue and red curves. (b) The time-dependent population of the MOs in the isolated monomer basis, Eq. (5). (H₂O 2a₁: black, H₂O 1b₁: cyan, H₂O 1b₂: grey, H₂O 3a₁: red, Ar 3s: orange, Ar 3p_x: green, Ar 3p_y: magenta, Ar 3p_z: blue) Insets show images of the MOs that are the dominant participants in the electron relaxation dynamics. The data shows a competition between hole transfer between Ar and H₂O and the expected ICD mechanism. The orbitals are plotted using Multiwfn.⁶⁰

effectively in a single cationic state, while the water molecule loses charge, is consistent with an ICD process and what was observed in the H₂O dimer, Fig. 2. However, the time-scale of ICD in the Ar-H₂O system is slower, taking on the order of 40 fs; this result intuitively makes sense as the strength of interaction between the non-hydrogen bonded Ar-H₂O system is weaker than in the H₂O dimer. Interestingly, in com-

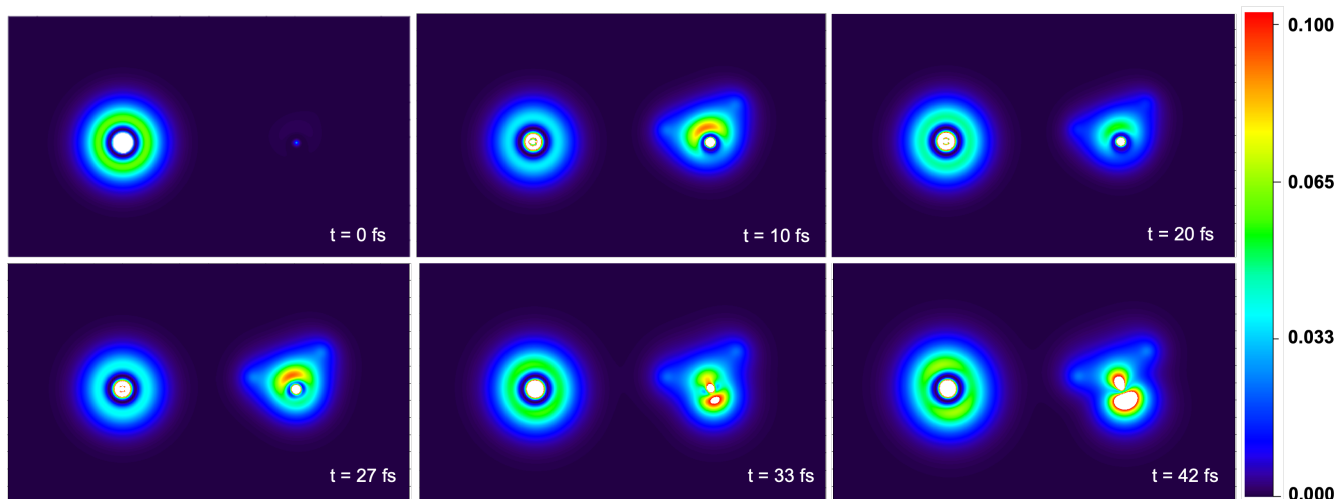


Figure 4: A heat-map of the time-dependent real-space hole density, Eq. (7), of the Ar-H₂O dimer. Specifically, the plot corresponds to the two-dimensional slice of the hole density corresponding to the plane of the Ar-H₂O dimer. The frames depict different times along the real-time TDDFT trajectory illustrating that there is oscillatory hole-transfer between Ar and H₂O s-like orbitals ($t = 0, 10, 20$, and 27 fs), followed by an ICD mechanism to yield p-like hole densities on both Ar and water ($t = 33$ and 42 fs). The hole density snapshots are plotted using Multiwfn.⁶⁰

parison to the H₂O dimer, Fig. 2(a) also indicates additional dynamics on the time-scale of the ICD process; the charge-loss on Ar and water oscillate out of phase with each other associated with charge transfer between the two species. The observed complicated dynamics and presence of ICD in the Ar-H₂O system is consistent with previous experimental work examining water clusters adsorbed on rare-gas surfaces.⁴

Further insight into the complex dynamics is provided in Fig. 3(b), which presents the time-dependent MO populations. The initial hole on the Ar 3s orbital (orange) first exhibits Rabi oscillations associated with hole transfer to the water 2a₁ MO (black), consistent with the charge transfer observed in Fig. 3(a). The Ar 3s orbital is then re-populated from electron density relaxing from the valence Ar 3p_x (blue) and 3p_z (green) orbitals, simultaneous with ionization of the valence water 3a₁ MO (red). In this context, we observe hole-transfer competing with the expected ICD process. The discovery and investigation of such competing pathways without any *a-priori* knowledge of which pathways are important illustrates the major benefit of real-time methodologies, especially in

more complex systems.

To illustrate that the observed hole-transfer dynamics is not simply an artifact of performing the analysis in the localized monomer basis, Fig. 4 presents the time-dependent real-space hole-density, which is insensitive to the choice of single-particle basis used to calculate the observable. We define the time-dependent real-space hole density as

$$\rho(\mathbf{r}, t) = \sum_{i=1}^{HOMO} (2 - \tilde{P}_{ii}(t)) |\tilde{\phi}_i(\mathbf{r})|^2 \quad (7)$$

where $\tilde{P}_{ii}(t)$ is the occupation number of i -th orbital at time t , and $\tilde{\phi}_i$ is the wavefunction of the i -th orbital. In the context of Eq. (7) and in Fig. 4, we specifically perform the sum in the basis of the MOs of the isolated monomers, Eq. (5); the sum runs up to the HOMO associated with the initial ground-state calculation. However, an analogous plot in a delocalized MO basis provided indistinguishable results to those observed in Fig. 4.

As shown in Fig. 4, the hole is initially located on Ar, exhibiting a spherical density pattern consistent with the 3s orbital. After 10 fs, the hole density partially transfers to the

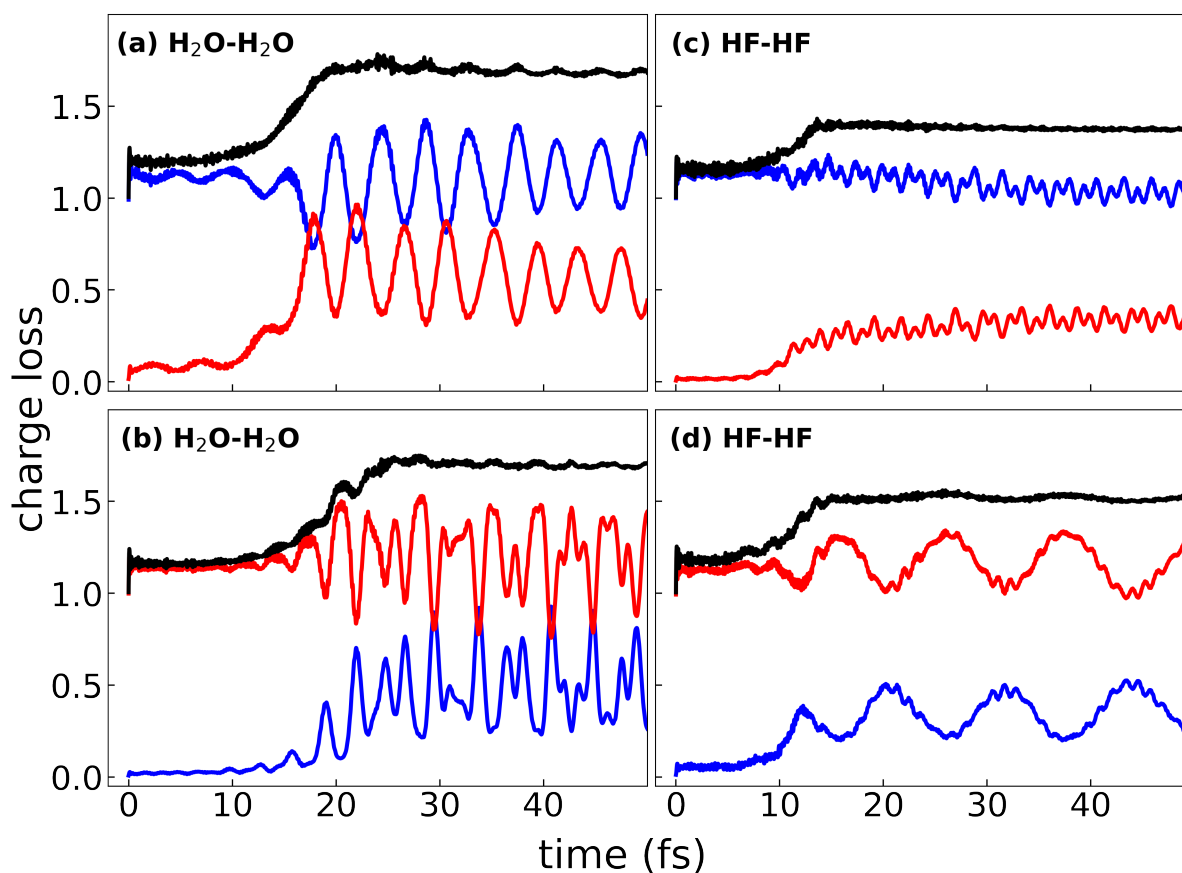


Figure 5: The time-dependent charge-loss, Eq. (6), for the H₂O-H₂O (left column) and HF-HF (right column) dimers. The upper row corresponds to generating the initial hole on the p-donor (blue), while the lower row corresponds to generating the initial hole on the p-acceptor (red). The total charge-loss of the dimer system (black) corresponds to the sum of the blue and red curves.

water molecule, exhibiting a distribution consistent with a localized 3a₁ orbital. The charge oscillation can then be observed in the snapshots at 20 fs and 27 fs. Following the charge oscillation, the hole density on Ar and on water change to distributions consistent with more p-like orbitals at 33 fs and finally at 42 fs, in agreement with the ICD process pictured in Fig. 3. The knowledge of the real-space density in comparison to the intermolecular distances may also provide a useful analysis tool as these parameters can have a strong influence on both the strength of the ICD coupling and the final Coulomb repulsion between species.⁴

Lastly, we examine the applicability of the developed real-time TD-DFFT methodology to correctly capture ICD dynamics in general systems. Figure 5, plots the time-dependent charge-loss the hydrogen-bonded dimers H₂O-H₂O (left) and HF-HF (right). The upper row

corresponds to generating the initial hole on the p-donor (blue), while the lower row corresponds to generating the initial hole on the p-acceptor (red). In general, we observe that the real-time TD-DFFT methodology correctly captures the ICD mechanism regardless of which monomer is initially ionized; the monomer with the initial hole stays in a cationic state, while the initial neutral monomer loses charge density associated with the secondary ionization process.

More specifically, both cases of H₂O-H₂O yield an ICD process that occurs on the order of 20-30 fs; this is consistent with previous kinetic energy release (KER) experiments that show roughly equal kinetic energy of the ionized secondary electron in both cases.² Similarly for HF-HF, both cases also show a clear ICD mechanism that occurs slightly faster, on the order of 15-20 fs, than the H₂O-H₂O dimer case. This behavior is consistent with results on the HF

trimer that indicate that ICD is possible both from a p-donor to a p-acceptor and the other way around.⁷

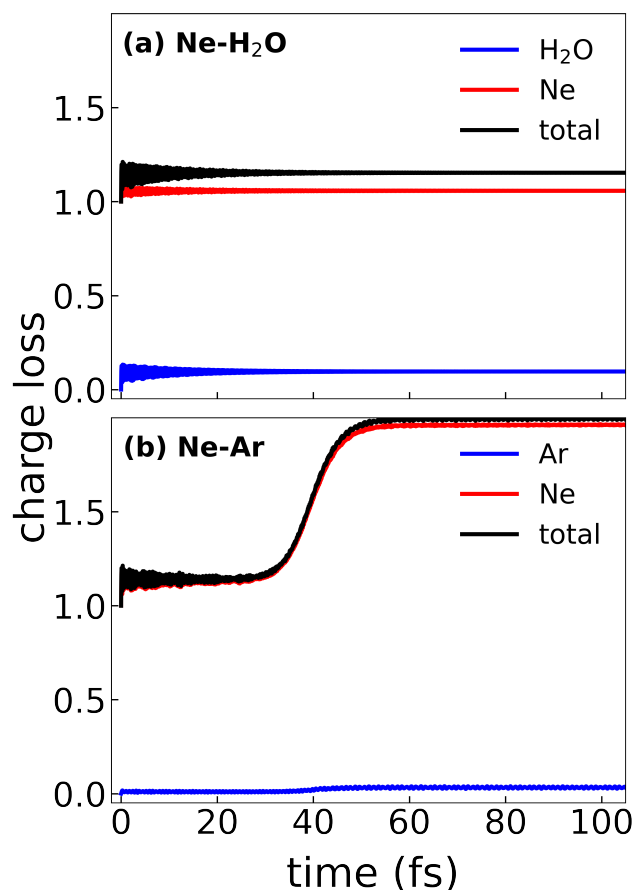


Figure 6: The time-dependent charge-loss, Eq. (6), for (a) the Ne-H₂O dimer and (b) the Ne-Ar dimer. In both cases, the initial hole is generated on Ne (blue) and the charge-loss of the other species is plotted in red. The total charge-loss of the dimer system (black) corresponds to the sum of the blue and red curves.

Figure 6 plots the time-dependent charge-loss for two more weakly bound systems, (a) Ne-H₂O and (b) Ne-Ar. In both cases, the initial hole is generated in the Ne 2s orbital (blue) and the charge loss of the other species is plotted in (red). It is expected that ICD should occur in Ne-H₂O,⁶¹ while ICD in Ne-Ar^{3,39,62–65} has been well established. However, Fig. 6 shows a break-down of the developed RT-TDDFT methodology in correctly predicting the ICD mechanism in these systems. For Ne-H₂O, Fig. 6(a), there is no energy exchange nor secondary ionization observed. For Ne-

Ar, Fig. 6(b), there is similarly no energy exchange and instead the Ne atom auto-ionizes, which should not be energetically feasible in this system. We attribute this breakdown to the weaker intermolecular forces in these systems, in comparison to the hydrogen bonded systems, that are more challenging for DFT to correctly capture.⁴⁴

In summary, we introduce a RT-TDDFT methodology to directly simulate the ultra-fast electron relaxation dynamics following an inner-valence ionization in real-time. The methodology involves utilizing (i) a complex absorbing potential (CAP) to remove the secondary ionized electron, (ii) a long-range corrected functional with diffuse basis functions, and (iii) a localized molecular orbital (MO) basis to perform the analysis. We examine a series of non-covalent bonded dimer systems, including HF-HF, H₂O-H₂O, Ar-H₂O, Ne-H₂O and Ne-Ar and show that our methodology can correctly capture the ICD mechanism in the hydrogen-bonded and Ar-H₂O systems, while the accuracy of the methodology breaks down in the more weakly bound Ne-H₂O and Ne-Ar systems. The presented methodology provides a useful tool to investigate competing electron relaxation pathways that is sufficiently efficient to examine complex systems.

Acknowledgement This study was financed in part by the U.S. Dept. of Energy, Office of Science, Basic Energy Sciences, Atomic, Molecular and Optical Sciences program, under Contract No. DE-FG02-02ER15337. J.X. Zhong Manis also acknowledges the U.S. Dept. of Energy, Office of Science Graduate Student Research (SCGSR) grant DE00000991SUS/GR10002881. J.S. Kretchmer gratefully acknowledges financial support from a start-up grant from the Georgia Institute of Technology. Computational resources were supported in part through research cyberinfrastructure resources and services provided by the Partnership for an Advanced Computing Environment (PACE) at the Georgia Institute of Technology, Atlanta, GA, USA.

Supporting Information Available

Details of the choice of functional, range-separation parameters, and basis; additional results comparing different bases; details of the choice and the values for the parameters of the complex absorbing potential

References

- (1) Wolf, T. J. A.; Paul, A. C.; Folkestad, S. D.; Myhre, R. H.; Cryan, J. P.; Berrah, N.; Bucksbaum, P. H.; Coriani, S.; Coslovich, G.; Feifel, R. et al. Transient resonant Auger–Meitner spectra of photoexcited thymine. *Faraday Discuss.* **2021**, *228*, 555–570.
- (2) Stoychev, S. D.; Kuleff, A. I.; Cederbaum, L. S. Intermolecular Coulombic Decay in Small Biochemically Relevant Hydrogen-Bonded Systems. *J. Am. Chem. Soc.* **2011**, *133*, 6817–6824.
- (3) Jahnke, T.; Hergenbahn, U.; Winter, B.; Dörner, R.; Frühling, U.; Demekhin, P. V.; Gokhberg, K.; Cederbaum, L. S.; Ehresmann, A.; Knie, A. et al. Interatomic and Intermolecular Coulombic Decay. *Chem. Rev.* **2020**, *120*, 11295–11369.
- (4) Grieves, G. A.; Orlando, T. M. Intermolecular Coulomb Decay at Weakly Coupled Heterogeneous Interfaces. *Phys. Rev. Lett.* **2011**, *107*, 016104.
- (5) Harbach, P. H. P.; Schneider, M.; Faraji, S.; Dreuw, A. Intermolecular Coulombic Decay in Biology: The Initial Electron Detachment from FADH⁻ in DNA Photolyases. *J. Phys. Chem. Lett.* **2013**, *4*, 943–949.
- (6) Cederbaum, L. S.; Zobeley, J.; Tarantelli, F. Giant Intermolecular Decay and Fragmentation of Clusters. *Phys. Rev. Lett.* **1997**, *79*, 4778–4781.
- (7) Zobeley, J.; Cederbaum, L. S.; Tarantelli, F. Highly excited electronic states of molecular clusters and their decay. *J. Chem. Phys.* **1998**, *108*, 9737–9750.
- (8) Zobeley, J.; Cederbaum, L. S.; Tarantelli, F. Intermolecular Coulombic Decay of Molecular Clusters: Identification of the Decay Mechanism Using a New Hole-Population Analysis. *J. Phys. Chem. A* **1999**, *103*, 11145–11160.
- (9) Kundu, S.; Hu, H.; Li, X.; Schaible, M.; Orlando, T. M. Electron scattering with ethane adsorbed on rare gas multilayers: Hole transfer, coulomb decay, and ion dissociation. *J. Chem. Phys.* **2023**, *158*.
- (10) Santra, R.; Cederbaum, L. S. Non-Hermitian electronic theory and applications to clusters. *Phys. Rep.* **2002**, *368*, 1–117.
- (11) Popov, A. Small helium clusters formation. *Int. J. Quantum Chem.* **2019**, *119*, e26045.
- (12) Jagau, T.-C. Theory of electronic resonances: fundamental aspects and recent advances. *Chem. Commun.* **2022**, *58*, 5205–5224.
- (13) Drescher, M.; Hentschel, M.; Kienberger, R.; Uiberacker, M.; Yakovlev, V.; Scrinzi, A.; Westerwalbesloh, Th.; Kleineberg, U.; Heinzmann, U.; Krausz, F. Time-resolved atomic inner-shell spectroscopy. *Nature* **2002**, *419*, 803–807.
- (14) Niikura, H.; Légaré, F.; Hasbani, R.; Bandrauk, A. D.; Ivanov, M. Yu.; Villeneuve, D. M.; Corkum, P. B. Sub-laser-cycle electron pulses for probing molecular dynamics. *Nature* **2002**, *417*, 917–922.
- (15) Niikura, H.; Villeneuve, D. M.; Corkum, P. B. Mapping Attosecond Electron Wave Packet Motion. *Phys. Rev. Lett.* **2005**, *94*, 083003.

- (16) Yabana, K.; Bertsch, G. F. Time-dependent local-density approximation in real time. *Phys. Rev. B* **1996**, *54*, 4484–4487.
- (17) Li, X.; Smith, S. M.; Markevitch, A. N.; Romanov, D. A.; Levis, R. J.; Schlegel, H. B. A time-dependent Hartree–Fock approach for studying the electronic optical response of molecules in intense fields. *Phys. Chem. Chem. Phys.* **2005**, *7*, 233–239.
- (18) Härtle, R.; Benesch, C.; Thoss, M. Multi-mode vibrational effects in single-molecule conductance: A nonequilibrium Green’s function approach. *Phys. Rev. B* **2008**, *77*, 205314.
- (19) Isborn, C. M.; Li, X.; Tully, J. C. Time-dependent density functional theory Ehrenfest dynamics: Collisions between atomic oxygen and graphite clusters. *J. Chem. Phys.* **2007**, *126*.
- (20) David, G.; Cohen, G.; Rabani, E. A semiclassical model for the non-equilibrium quantum transport of a many-electron Hamiltonian coupled to phonons. *Mol. Phys.* **2012**, 743–750.
- (21) Li, B.; Levy, T. J.; Swenson, D. W. H.; Rabani, E.; Miller, W. H. A Cartesian quasi-classical model to nonequilibrium quantum transport: The Anderson impurity model. *J. Chem. Phys.* **2013**, *138*.
- (22) Thiel, W. Semiempirical quantum–chemical methods. *WIREs Comput. Mol. Sci.* **2014**, *4*, 145–157.
- (23) Cohen, G.; Gull, E.; Reichman, D. R.; Millis, A. J. Taming the Dynamical Sign Problem in Real-Time Evolution of Quantum Many-Body Problems. *Phys. Rev. Lett.* **2015**, *115*, 266802.
- (24) Goings, J. J.; Lestrangle, P. J.; Li, X. Real-time time-dependent electronic structure theory. *WIREs Comput. Mol. Sci.* **2018**, *8*, e1341.
- (25) Wang, Y.-S.; Zhou, X.; Tomko, J. A.; Giri, A.; Hopkins, P. E.; Prezhdo, O. V. Electron–Phonon Relaxation at Au/Ti Interfaces Is Robust to Alloying: Ab Initio Nonadiabatic Molecular Dynamics. *J. Phys. Chem. C* **2019**, *123*, 22842–22850.
- (26) Baiardi, A.; Reiher, M. Large-Scale Quantum Dynamics with Matrix Product States. *J. Chem. Theory Comput.* **2019**, *15*, 3481–3498.
- (27) Koulias, L. N.; Williams-Young, D. B.; Nascimento, D. R.; Deprince, A. E. I.; Li, X. Relativistic Real-Time Time-Dependent Equation-of-Motion Coupled-Cluster. *J. Chem. Theory Comput.* **2019**, *15*, 6617–6624.
- (28) Chatterjee, S.; Makri, N. Real-Time Path Integral Methods, Quantum Master Equations, and Classical vs Quantum Memory. *J. Phys. Chem. B* **2019**, *123*, 10470–10482.
- (29) Wang, Y.-S.; Nijjar, P.; Zhou, X.; Bondar, D. I.; Prezhdo, O. V. Combining Lindblad Master Equation and Surface Hopping to Evolve Distributions of Quantum Particles. *J. Phys. Chem. B* **2020**, *124*, 4326–4337.
- (30) Li, W.; Ren, J.; Shuai, Z. Finite-Temperature TD-DMRG for the Carrier Mobility of Organic Semiconductors. *J. Phys. Chem. Lett.* **2020**, *11*, 4930–4936.
- (31) Zhou, G.; Lu, G.; Prezhdo, O. V. Modeling Auger Processes with Nonadiabatic Molecular Dynamics. *Nano Lett.* **2021**, *21*, 756–761.
- (32) Jiang, K.; Pavanello, M. Time-dependent orbital-free density functional theory: Background and Pauli kernel approximations. *Phys. Rev. B* **2021**, *103*, 245102.
- (33) Church, M. S.; Rubenstein, B. M. Real-time dynamics of strongly correlated fermions using auxiliary field quantum Monte Carlo. *J. Chem. Phys.* **2021**, *154*.

- (34) Cortes, C. L.; DePrince, A. E.; Gray, S. K. Fast-forwarding quantum simulation with real-time quantum Krylov subspace algorithms. *Phys. Rev. A* **2022**, *106*, 042409.
- (35) Wang, Z.; Peyton, B. G.; Crawford, T. D. Accelerating Real-Time Coupled Cluster Methods with Single-Precision Arithmetic and Adaptive Numerical Integration. *J. Chem. Theory Comput.* **2022**, *18*, 5479–5491.
- (36) Zheng, Z.; Shi, Y.; Zhou, J.-J.; Prezhdo, O. V.; Zheng, Q.; Zhao, J. Ab initio real-time quantum dynamics of charge carriers in momentum space. *Nat. Comput. Sci.* **2023**, *3*, 532–541.
- (37) Yehorova, D.; Kretchmer, J. S. A multi-fragment real-time extension of projected density matrix embedding theory: Non-equilibrium electron dynamics in extended systems. *J. Chem. Phys.* **2023**, *158*.
- (38) Peyton, B. G.; Wang, Z.; Crawford, T. D. Reduced Scaling Real-Time Coupled Cluster Theory. *J. Phys. Chem. A* **2023**, *127*, 8486–8499.
- (39) Kuleff, A. I.; Cederbaum, L. S. Tracing Ultrafast Interatomic Electronic Decay Processes in Real Time and Space. *Phys. Rev. Lett.* **2007**, *98*, 083201.
- (40) Zhou, J.; He, C.; Liu, M.-M.; Wang, E.; Jia, S.; Dorn, A.; Ren, X.; Liu, Y. Real-time observation of ultrafast molecular rotation in weakly bound dimers. *Phys. Rev. Res.* **2021**, *3*, 023050.
- (41) Krishtal, A.; Ceresoli, D.; Pavanello, M. Subsystem real-time time dependent density functional theory. *J. Chem. Phys.* **2015**, *142*.
- (42) Shi, R.; Fang, Q.; Vasenko, A. S.; Long, R.; Fang, W.-H.; Prezhdo, O. V. Structural Disorder in Higher-Temperature Phases Increases Charge Carrier Lifetimes in Metal Halide Perovskites. *J. Am. Chem. Soc.* **2022**, *144*, 19137–19149.
- (43) Svoboda, O.; Hollas, D.; Ončák, M.; Slavíček, P. Reaction selectivity in an ionized water dimer: nonadiabatic ab initio dynamics simulations. *Phys. Chem. Chem. Phys.* **2013**, *15*, 11531–11542.
- (44) Chalabala, J.; Uhlig, F.; Slavíček, P. Assessment of Real-Time Time-Dependent Density Functional Theory (RT-TDDFT) in Radiation Chemistry: Ionized Water Dimer. *J. Phys. Chem. A* **2018**, *122*, 3227–3237.
- (45) Andrade, X.; Alberdi-Rodriguez, J.; Strubbe, D. A.; Oliveira, M. J. T.; Nogueira, F.; Castro, A.; Muguerza, J.; Arruabarrena, A.; Louie, S. G.; Aspuru-Guzik, A. et al. Time-dependent density-functional theory in massively parallel computer architectures: the octopus project. *J. Phys.: Condens. Matter* **2012**, *24*, 233202.
- (46) Fischer, S. A.; Cramer, C. J.; Govind, N. Excited-State Absorption from Real-Time Time-Dependent Density Functional Theory: Optical Limiting in Zinc Phthalocyanine. *J. Phys. Chem. Lett.* **2016**, *7*, 1387–1391.
- (47) Fernando, R. G.; Balhoff, M. C.; Lopata, K. X-ray Absorption in Insulators with Non-Hermitian Real-Time Time-Dependent Density Functional Theory. *J. Chem. Theory Comput.* **2015**, *11*, 646–654.
- (48) Lane, J. R. CCSDTQ Optimized Geometry of Water Dimer. *J. Chem. Theory Comput.* **2013**, *9*, 316–323.
- (49) Peterson, K. A.; Dunning, T. H. Benchmark calculations with correlated molecular wave functions. VII. Binding energy and structure of the HF dimer. *J. Chem. Phys.* **1995**, *102*, 2032–2041.
- (50) Weigend, F.; Ahlrichs, R. Balanced basis sets of split valence, triple zeta valence and quadruple zeta valence quality for H to Rn: Design and assessment of accuracy.

- Phys. Chem. Chem. Phys.* **2005**, *7*, 3297–3305.
- (51) Maroulis, G.; Haskopoulos, A. Interaction induced (hyper)polarizability in Ne...Ar. *Chem. Phys. Lett.* **2002**, *358*, 64–70.
- (52) Rohrdanz, M. A.; Herbert, J. M. Simultaneous benchmarking of ground- and excited-state properties with long-range-corrected density functional theory. *J. Chem. Phys.* **2008**, *129*.
- (53) Lopata, K.; Govind, N. Near and Above Ionization Electronic Excitations with Non-Hermitian Real-Time Time-Dependent Density Functional Theory. *J. Chem. Theory Comput.* **2013**, *9*, 4939–4946.
- (54) Bruner, A.; Hernandez, S.; Mauger, F.; Abanador, P. M.; LaMaster, D. J.; Gaarde, M. B.; Schafer, K. J.; Lopata, K. Attosecond Charge Migration with TDDFT: Accurate Dynamics from a Well-Defined Initial State. *J. Phys. Chem. Lett.* **2017**, *8*, 3991–3996.
- (55) Dunning, T. H. Gaussian basis sets for use in correlated molecular calculations. I. The atoms boron through neon and hydrogen. *J. Chem. Phys.* **1989**, *90*, 1007–1023.
- (56) Woon, D. E.; Dunning, T. H. Gaussian basis sets for use in correlated molecular calculations. IV. Calculation of static electrical response properties. *J. Chem. Phys.* **1994**, *100*, 2975–2988.
- (57) Aprà, E.; Bylaska, E. J.; de Jong, W. A.; Govind, N.; Kowalski, K.; Straatsma, T. P.; Valiev, M.; van Dam, H. J. J.; Alexeev, Y.; Anchell, J. et al. NWChem: Past, present, and future. *J. Chem. Phys.* **2020**, *152*.
- (58) Lopata, K.; Govind, N. Modeling Fast Electron Dynamics with Real-Time Time-Dependent Density Functional Theory: Application to Small Molecules and Chromophores. *J. Chem. Theory Comput.* **2011**, *7*, 1344–1355.
- (59) Szabo, A.; Ostlund, N. S. *Modern quantum chemistry: introduction to advanced electronic structure theory*; Courier Corporation, 2012.
- (60) Lu, T.; Chen, F. Multiwfn: A multifunctional wavefunction analyzer. *J. Comput. Chem.* **2012**, *33*, 580–592.
- (61) Ghosh, A.; Pal, S.; Vaval, N. Study of interatomic Coulombic decay of Ne(H₂O)_n (n = 1,3) clusters using equation-of-motion coupled-cluster method. *J. Chem. Phys.* **2013**, *139*.
- (62) Lundwall, M.; Pokapanich, W.; Bergersen, H.; Lindblad, A.; Rander, T.; Öhrwall, G.; Tchapyguine, M.; Barth, S.; Hergenbahn, U.; Svensson, S. et al. Self-assembled heterogeneous argon/neon core-shell clusters studied by photoelectron spectroscopy. *J. Chem. Phys.* **2007**, *126*.
- (63) Zobeley, J.; Santra, R.; Cederbaum, L. S. Electronic decay in weakly bound heteroclusters: Energy transfer versus electron transfer. *J. Chem. Phys.* **2001**, *115*, 5076–5088.
- (64) Scheit, S.; Averbukh, V.; Meyer, H.-D.; Zobeley, J.; Cederbaum, L. S. Interatomic Coulombic decay in a heteroatomic rare gas cluster. *J. Chem. Phys.* **2006**, *124*.
- (65) Barth, S.; Marburger, S.; Joshi, S.; Ulrich, V.; Kugeler, O.; Hergenbahn, U. Interface identification by non-local autoionization transitions. *Phys. Chem. Chem. Phys.* **2006**, *8*, 3218–3222.

Supporting Information: Modeling intermolecular Coulombic decay with non-Hermitian real-time time-dependent density functional theory

Yi-Siang Wang, James X. Zhong Manis, Matthew C. Rohan, Thomas M.
Orlando, and Joshua S. Kretchmer*

*School of Chemistry and Biochemistry, Georgia Institute of Technology, Atlanta, GA
30332, USA*

E-mail: jkretchmer@gatech.edu

Initialization of the hole

We use the following procedure to generate the 1-electron reduced density matrix (1RDM), \mathbf{P} , that accounts for the initial ionization event: *(i)* We manually form a diagonal 1RDM, \mathbf{P}_{MO} , with the diagonal elements given by either 2 or 0 corresponding to the occupied or virtual molecular orbital (MO)s. However, we change the diagonal element for the MO that corresponds to the ionized MO to 1 instead of 2. The MO indices correspond to those obtained from the ground-state DFT calculation on the dimer. *(ii)* This diagonal 1RDM is then rotated into the AO basis using

$$\mathbf{P} = \mathbf{C}\mathbf{P}_{\text{MO}}\mathbf{C}^\dagger, \quad (1)$$

where \mathbf{C} corresponds to the MO coefficient matrix in the atomic orbital (AO) basis obtained from the ground-state DFT calculation on the dimer. (iii) This final 1RDM, \mathbf{P} , is then used as the starting point for the subsequent real-time time-dependent density functional theory (RT-TDDFT) calculation.

Choice of range-separation parameter

In this work we use the tuned long-range corrected LC-PBE* functional. We use a previously developed procedure to obtain a good choice of the range-separation parameter μ by minimizing the difference between the Koopmans' ionization potential and the true ionization potential.^{1,2} This is done by minimizing the following object function

$$J(\mu) = |IP_{\text{SCF}}(\mu) - IP_{\text{Koopman}}(\mu)| = |E_{\text{SCF}}^{\text{cation}}(\mu) - E_{\text{SCF}}^{\text{neutral}}(\mu) + \varepsilon_{\text{HOMO}}^{\text{neutral}}(\mu)|, \quad (2)$$

where the subscript SCF corresponds to a ground-state DFT energy and $\varepsilon_{\text{HOMO}}^{\text{neutral}}(\mu)$ is the energy of the HOMO from the neutral ground-state DFT calculation.

This procedure is performed for the various molecules studied in the manuscript. Specifically, the range-separation parameter is chosen for each molecule based on isolated monomer calculations. For the dimer systems, the range-separation parameter is chosen to be that of the monomer value associated with the target molecule. The final values of the range-separation parameter is provided in Table 1.

Table 1: The values of the range-separation parameter (μ), and the CAP parameters ε_0 and ζ . The molecule refers to the target molecule in each dimer.

Molecule	μ	ε_0	ζ
p-donor H ₂ O	0.51	0.047	0.5
p-acceptor H ₂ O	0.51	0.047	0.5
p-donor HF	0.64	0.024	0.1
p-acceptor HF	0.64	0.024	0.2
Ar	0.57	0.079	0.5

Choice of parameters in the complex absorbing potential

The diagonal damping matrix, D , used in the complex absorbing potential (CAP) has elements given by

$$\gamma_i = \begin{cases} 0, & \text{if } \varepsilon_i - \varepsilon_0 < 0 \\ \gamma_0 e^{-\xi(\varepsilon_i - \varepsilon_0)}, & \text{if } \varepsilon_i - \varepsilon_0 > 0 \end{cases} \quad (3)$$

which corresponds to Eq. (4) in the main text. To obtain the specific values for the terms γ_0 , ξ , and ε_0 used to define the strength of the damping matrix, we follow an analogous protocol as employed in the context of spectroscopic calculations.^{1,3}

First, the value of γ_0 is always chosen to be 1 Ha, and the value of γ_i is capped to a maximum value of 100 Ha as was done previously.³

The value of the cut-off energy, ε_0 , is chosen to partition the virtual orbitals into a set of bound or continuum orbitals based on their energy in comparison the following estimate of the electron affinity:³

$$EA_1 = E^{anion} - E^{neutral} \quad (4)$$

$$EA_k \simeq EA_1 + \nu_{k-1} \quad k = 2, 3, \dots \quad (5)$$

where ν_k corresponds to the k th TDDFT excitation of the anion. For a given value of k , EA_k and EA_{k+1} will switch from negative to positive. The value of ε_0 is chosen to match the interpolated value between ν_k and ν_{k+1} , such that the electron affinity equals zero. This procedure is performed on an isolated monomer and, analogous to the range-separation parameter, the value for a dimer system is chosen to be that of the monomer value associated with the target molecule. The values for each monomer are provided in Table 1.

Previous work focusing on spectroscopic calculations chose the value of the exponential decay parameter, ξ , large enough to remove spurious peaks in the spectra, but not so high to begin to alter the gross features. We take a similar tactic in the context of the calculations presented in this work. Specifically, we choose ξ to be as large as possible, but not so large

to introduced artificial over-ionization of the system. A signature of artificial ionization is associated with the ionization of the trigger molecule from arbitrary MOs, which should not be an energetically feasible process in any of the systems studied herein. This is in comparison to the clean change in MO occupation associated with the intermolecular Coulombic decay (ICD) process presented in the main text. The final values of ξ are presented in Table 1.

Functional/basis set dependence

To choose a proper functional/basis set combination for capturing the ICD dynamics, we tested the following four combinations: LC-PBE*/aDZ-aDZ, LC-PBE*/aDZ-daDZ, LC-PBE*/daDZ-daDZ, and CAM-B3LYP/daDZ-daDZ on the water dimer with the p-donor acting as the trigger molecule. Here, aDZ and d-aDZ refer to the aug-cc-pVDZ and d-aug-cc-pVDZ basis sets, while the notation basis1-basis2 corresponds to using basis1 for the trigger molecule and basis2 for the target molecule. Fig. 1 plots the charge loss on both water molecules along with the total charge loss for all four combinations. We observe analogous behavior in all four plots in terms of both the time-scale of the ICD process along with the final plateau values of the charge-loss on both water molecules. The exact nature of the high-frequency oscillations after ~ 20 fs differ slightly between the different choices. However, given that these oscillations are most likely not physically relevant, we use LC-PBE*/aDZ-daDZ for all systems in our study.

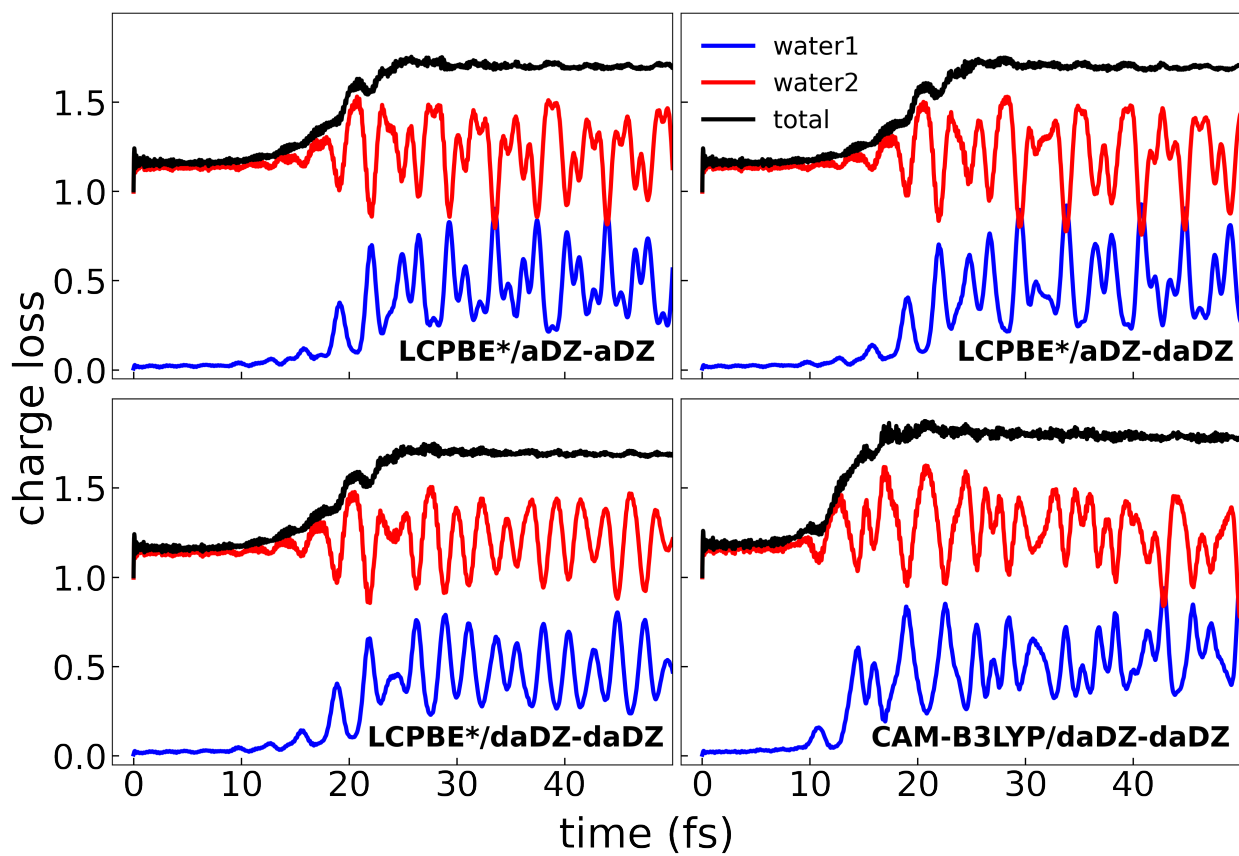


Figure 1: The time-dependent charge loss for the water dimer using different functional/basis set combinations.

References

- (1) Lopata, K.; Govind, N. Near and Above Ionization Electronic Excitations with Non-Hermitian Real-Time Time-Dependent Density Functional Theory. *J. Chem. Theory Comput.* **2013**, *9*, 4939–4946.
- (2) Lopata, K.; Govind, N. Modeling Fast Electron Dynamics with Real-Time Time-Dependent Density Functional Theory: Application to Small Molecules and Chromophores. *J. Chem. Theory Comput.* **2011**, *7*, 1344–1355.
- (3) Fernando, R. G.; Balhoff, M. C.; Lopata, K. X-ray Absorption in Insulators with Non-Hermitian Real-Time Time-Dependent Density Functional Theory. *J. Chem. Theory Comput.* **2015**, *11*, 646–654.